Annals of Biomedical Engineering, Vol. 37, No. 4, April 2009 (© 2009) pp. 722–736
DOI: 10.1007/s10439-009-9642-0

Biomolecular Transport Through Hemofiltration Membranes

A. T. Conlisk,[1] Subhra Datta,[1] William H. Fissell,[2] and Shuvo Roy[3,4]

[1]Department of Mechanical Engineering, The Ohio State University, 201 West 19th Avenue, Columbus, OH 43210, USA; [2]Departments of Nephrology and Hypertension and Biomedical Engineering, Cleveland Clinic, 9500 Euclid Avenue, Cleveland, OH 44195, USA; [3]Department of Biomedical Engineering, Cleveland Clinic, 9500 Euclid Avenue, Cleveland, OH 44195, USA; and [4]Department of Bioengineering and Therapeutic Sciences, University of California, San Francisco, CA 94158, USA

(*Received 1 August 2008; accepted 12 January 2009; published online 30 January 2009*)

Abstract—A theoretical model for filtration of large solutes through a pore in the presence of transmembrane pressures, applied/induced electric fields, and dissimilar interactions at the pore entrance and exit is developed to characterize and predict the experimental performance of a hemofiltration membrane with nanometer scale pores designed for a proposed implantable Renal Assist Device (RAD). The model reveals that the sieving characteristics of the membrane can be improved by applying an external electric field, and ensuring a smaller ratio of the pore-feed and pore-permeate equilibrium partitioning coefficients when diffusion is present. The model is then customized to study the sieving characteristics for both charged and uncharged solutes in the slit-shaped nanopores of the hemofiltration device for the RAD. The effect of streaming potential or induced fields are found to be negligible under representative operating conditions. Experimental data on the sieving coefficient of bovine serum albumin, carbonic anhydrase and thyroglobulin are reported and compared with the theoretical predictions. Both steric and electrostatic partitioning are considered and the comparison suggests that in general electrostatic effects are present in the filtration of proteins though some data, particularly those recorded in a strongly hypertonic solution (10× PBS), show better agreement with the steric partitioning theory.

Keywords—Hemofiltration, Synthetic nanopore membrane, Renal replacement therapy, Sieving coefficient, Kidney.

INTRODUCTION

A semipermeable membrane allows the passage of certain molecules while restricting the passage of others and is an important component of filtration mechanisms in nature[12,34,47] as well as technology.[53] While most semipermeable membranes to date employ circular pores, membranes with slit shaped pore cross-sections have recently received attention owing to its greater ease of fabrication utilizing silicon nano-electromechanical-systems (NEMS) technology[15,33] and higher intrinsic hydraulic permeability[18] than circular pore membranes. The latter characteristic makes slit pore membranes attractive for filtration volume intensive tasks like the *in vivo* replacement of renal function.[24]

The work described in this paper has been pursued with the objective of modeling the transport of large macromolecules within nanopores (~10 nm) of a synthetic hemofiltration membrane.[16] This hemofiltration membrane is a key subunit of an implantable Renal Assist Device (RAD)[16] conceptualized to substitute kidney function *in vivo* during renal replacement therapy of patients suffering from end stage renal disease (ESRD) and acute renal failure (ARF) (conditions afflicting hundreds of thousands of people in the United States[24]). A hemofiltration membrane more accurately mimics the native kidney function[24] than *ex vivo* dialysis membranes by using a transmembrane pressure to control both permeate and solute fluxes, and not relying on solute concentration differences across the membrane for the success of its operation. A consequence of the predominantly convective nature of the solute fluxes during hemofiltration is a better clearance of middle molecules (0.3–12 kDa) such as β_2-microglobulin (11 kDa) and large molecular weight toxins that are extremely slow to diffuse across a dialysis membrane.[35] In conjunction with suitable tissue engineering and microelectromechanical system (MEMS) based control strategies, hemofiltration membranes are promising candidates for use in a continuously operating and implantable artificial kidney[16,24] of which the RAD will be a first generation. However, it is necessary to ensure a highly restricted passage through the membrane of essential proteins like serum albumin (desired sieving coefficient ~ 10^{-2}%[24]). Therefore, a broader goal of this work is to

Address correspondence to Subhra Datta, Department of Mechanical Engineering, The Ohio State University, 201 West 19th Avenue, Columbus, OH 43210, USA. Electronic mail: datta.20@osu.edu, conlisk.1@osu.edu

0090-6964/09/0400-0722/0 © 2009 Biomedical Engineering Society

identify the conditions necessary to achieve the desired selectivity utilizing a hemofiltration membrane with *slit pores*.

A conceptual diagram of the envisaged implanted form of the RAD is shown in Fig. 1. The RAD will consist of a hemofiltration module and a cell bioreactor module to replace the filtration and readsorption tasks of a kidney, respectively.[16,24] The final device will be a compact biocompatible cartridge handling afferent and efferent streams of blood and an exit stream that drains into the bladder.

Figure 2a shows a scanning electron micrograph of a typical membrane used for hemofiltration in the RAD.[18] A section through the line segment AB in the left pane is shown in the center pane. The right pane is a magnified view of the same section showing a nanopore. Figures 2b and 2c show the side and end views of the membrane schematically. Figure 2d shows an individual nanopore of width $2h$ confining a molecule of radius a. The membrane consists of a large number of nanopores (~10^4) and connects an upstream feed microchannel where the average flow speed is U_F to a downstream permeate microchannel where the average flow speed is U_P (Fig. 2b). The characteristic dimensions of the feed and permeate channel are on the scale of millimeters and the flow rate in the feed channel is of the order of milliliters per second; an external pump is used to drive this flow past the membrane.[18] The flow speed U_P in the permeate channel is solely due to permeation of the feed solution through the membrane pores and is not imposed externally as in dialysis or hemodiafiltration.[18] The flow across the nanopore membrane is driven by a transmembrane pressure drop of ~1–2 psi established between the feed and permeate solution (Fig. 2b). In Fig. 2c, the flow is normal to the plane of paper in the end view of the membrane. Figure 2d shows the geometry of an individual nanopore and the coordinate system chosen for the theoretical model.

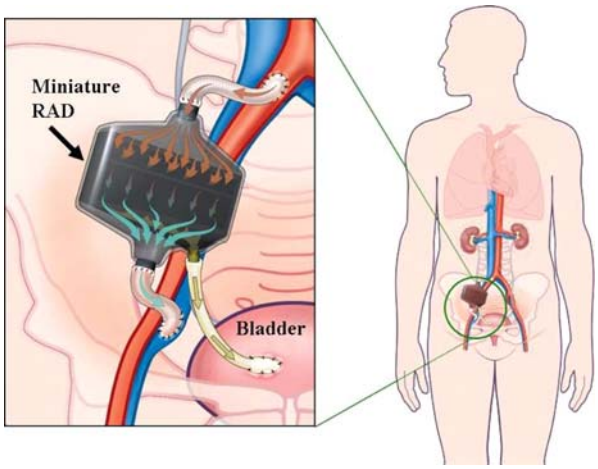


FIGURE 1. A Miniaturized Renal Assist Device (RAD) surgically implanted into a soft tissue pocket near the pelvis through vascular anastomoses and draining into the bladder through a urinary conduit.

To simplify the theoretical problem, the pores are assumed to be straight, nonintersecting and of uniform width. The width $2h$ of each nanopore is ~10 nm; for example, $2h = 8$ nm for the membranes described by Fissell *et al.*[18] As evident from Figs. 2b and 2c the other dimensions of the nanopore are large enough for the pore to be treated as a slit. A hemofiltration chip in the first generation of the RAD[18] consists of an array of several (five to nine) such membranes. The chip is fabricated using a state-of-the-art in nanofabrication technology that involves deposition of a sacrificial layer of SiO_2 for the definition of nanopore size and can be controlled precisely enough to result in a nearly monodisperse pore size distribution (<1% variation across the chip) for 5 nm pores.[16,18] The chip fabrication and the experimental setup for a hemofiltration experiment are described in more detail in Fissell *et al.*[18]

The sieving coefficient (S) of a solute with concentration C_P in the permeate channel and C_F in the feed channel is defined by $S = C_P/C_F$. Small S values are desirable and the inverse of the sieving coefficient $1/S$ can be considered a quantitative measure of its selectivity.[36] In this work, we will concentrate on obtaining concentration distributions within each pore and the corresponding sieving coefficients. Therefore, 'microscale' variables such as mean flow velocity $\bar{u}$ within a pore rather than the membrane scale variables such as permeate flux J_v will be used.[53]

Pore level transport phenomena in the presence of both applied pressure drops and applied/induced electric fields are investigated in this work. The effect of dissimilar interactions at the entrance and exit of the pores on solute distributions and solute selectivity of the pore is modeled, and an explanation of the sensitivity of experimental observations to permeate side conditions observed in the recent experiments of Roy and Fissell[46] is provided. New experimental results on protein filtration with the synthetic nanopore membrane for the RAD are reported and good agreement is obtained with the theoretical predictions.

An electric field is induced naturally in any charged pore that carries flow generated by other motive forces like pressure drop; this phenomenon is known as streaming potential.[14] The contribution of streaming potential in pressure-driven nanofiltration with slit-pore membranes will be studied for the first time in the literature. Unlike previous work,[29,43] both concentration distributions along the pore and sieving coefficients are derived, and the combined effects of electric fields and pore entrance and exit phenomena are

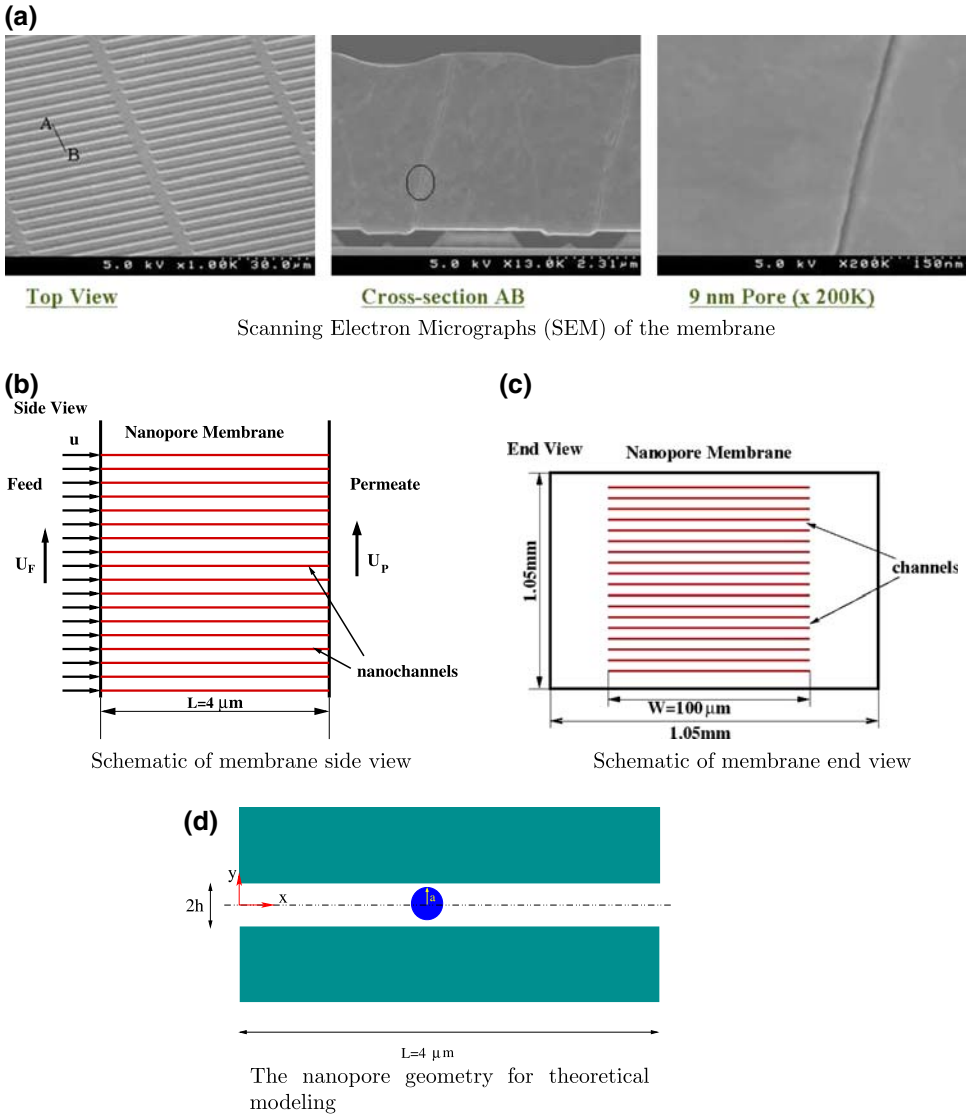


FIGURE 2. A synthetic nanopore membrane for the proposed RAD.[18] (a) Scanning Electron Micrographs (SEM) of a representative membrane used in the experiments; the top view is on the first pane from the left, the sectional view through the line segment AB (in the top view) is shown in the center pane, and a 9 nm nanopore is visible in the right pane, which is a magnified version of the center pane; (b) and (c) schematic representation of membrane side and end views, respectively; (d) shows a solute molecule of Stokes–Einstein radius *a* is within a uniform nanopore of width 2*h*.

studied to reveal novel experimental approaches for improving membrane performance. Most of the work in the literature has focused on circular pores[9,10,43,53] and both experimental data and models applicable to membranes employing slit shaped pores similar to those reported in this work are scarce.

In section "Modeling of Pore Scale Hindered Transport," a model for the hindered transport of a macromolecular solute in the presence of flow, wall charges and applied/induced electrostatic fields is developed in order to characterize pore scale nanofiltration performance in a general manner. In section "Application to Hemofiltration," this model is customized to the slit-pore geometry, pore-bulk equilibrium partitioning behavior for both charged and uncharged solutes and operating conditions appropriate to the hemofiltration membrane for the proposed RAD during filtration of uncharged and charged molecules. Section "Modeling of Pore Scale Hindered Transport" results in recommendations of experimental significance to the design and characterization of membrane-based ultrafiltration/nanofiltration processes, by phenomenologically taking into consideration (a) arbitrary geometrical and physical characteristics of the membrane pore, solute, and their mutual interaction and (b) either pressure/voltage driven ultrafiltration;

the theoretical results of section "Modeling of Pore Scale Hindered Transport" should therefore be much broader in scope than merely the applications of interest in this study. Section "Application to Hemofiltration" studies the results of section "Modeling of Pore Scale Hindered Transport" in the more specialized context of the pressure-driven ultrafiltration application of interest to the development of hemofilters for the RAD. To that end, in section "Application to Hemofiltration," concrete theoretical specifications are made for the effects of factors that are important in the experiments toward the hemofilter development, such as the shape of the pore, the charge of the pore and the solute and the monodisperse/polydisperse nature of the solute. The theoretical model of section "Modeling of Pore Scale Hindered Transport" is also simplified in section "Application to Hemofiltration" for the purpose of experimental application, by providing arguments to neglect factors, such as streaming potential, that are estimated to be quantitatively insignificant in the experiments. Finally, section "Application to Hemofiltration" describes new ultrafiltration experiments on retention of proteins conducted with a tangential flow filtration setup[18] and membranes with slit-shaped pores similar to that shown in Fig. 2a and performs a comparison of the experimental results with the specialized sieving theory of charged/uncharged solutes in slit-shaped pores. Conclusions and scope for future research are discussed in section "Conclusions".

MODELING OF PORE SCALE HINDERED TRANSPORT

The pores are taken to be straight channels connecting the side of the membrane in contact with the feed solution to that in contact with the permeate. The model developed in this section is appropriate for slit pores as well as circular pores[6,10] and is based on operating conditions such as applied electric fields that are more general than that in the experiments of Fissell *et al.*[18] In a later section we will specialize the model to the proposed RAD which utilizes slit pore membranes (Fig. 2).

Governing Equations

The solute molecules of interest in hemofiltration (e.g., proteins like serum albumin) have characteristic diameters that are comparable to the nanopore width (~10 nm). This renders entrance into the pore from a bulk solution unfavorable and exit from the pore favorable. Inside the pore, the prevalent rates of diffusion and convection of solutes are different from that when the solute is not constrained by walls; this phenomenon is known as hindered transport. The diffusion coefficient of the solute in an unbounded solution D can be scaled by a 'diffusional hindrance factor' $K_d < 1$ to obtain the hindered diffusion coefficient $K_d D$ in the pore. The solute is convected at a speed $K_c\bar{u}$ different from the local area averaged axial velocity $\bar{u}$ in the pore. The factor K_c is known as the 'convection hindrance factor'.

The local mole fraction of the biomolecular solute is given by X at the point where its centroid is located. Only the axial variation of the solute concentration is of interest for understanding pore filtration and selectivity performance. Moreover, the cross-sectional variation of concentration can be derived from the axial variation, once the latter is known.[6,10] It will therefore suffice to use a transport equation for the area averaged solute mole fraction $\bar{X}$. The formal method of constructing an area averaged equation for the solute concentration is shown in Brenner and Gaydos.[6] Neglecting Taylor dispersion effects,[6,11] the distribution of $\bar{X}$ indicates a balance of hindered diffusion, convection, and migration in the following form:

$$\frac{dJ}{dx} = 0 \tag{1a}$$

$$J = K_c\left[-\frac{1}{Pe_H}\left(\frac{\partial \bar{X}}{\partial x} - zE_x\bar{X}\right) + \bar{u}\bar{X}\right] \tag{1b}$$

Denoting dimensional quantities with asterisks, the dimensionless distance along the pore, the dimensionless velocity and electric field are $x = x^*/L$, $u = u^*/U_0$ and $E_x = E_x^* L/\phi_0$. L is the length of the membrane and $\bar{u}$ is the cross-sectional average of the flow velocity u. $J = J^*/(\bar{u}^* X_0)$ is the dimensionless solute flux. The velocity scale is $U_0 = h^2\Delta P/2\,\mu L$ and can be interpreted as the centerline velocity of a purely pressure-driven flow of a liquid of viscosity μ under the transmembrane pressure difference $P_F - P_P = \Delta P$, where F denotes feed and P denotes permeate. The potential scale $\phi_0 = RT/F \simeq 26$ mV at $T = 298$ K. Here, R is the universal gas constant, F is the Faraday's constant, and T is the temperature. $Pe_H = K_c U_0 L/K_d D$ is the 'hindered transport Peclet number' and can be interpreted as the characteristic ratio of axial convection speed to axial diffusion speed of a solute constrained by the pore. A steady state in the pore has been assumed in formulating Eq. (1).

In Eq. (1), the axial electrophoretic motion of the solute in the presence of applied or induced electric fields has been treated for simplicity as an ionic electromigration of an ion of valence z; for example $z \simeq -20$ for bovine serum albumin (BSA) at physiological pH[42]; another possibility is to utilize electrophoretic mobility

based approach.[43] In either approach, the flux is proportional to the applied electric field and to avoid introducing another unknown parameter for 'hindered electrophoresis'[43] the Nernst Einstein relationship for connecting mobility to diffusion coefficients is invoked.[6]

Boundary Conditions

In order to solve for the concentration distribution of the solute within a slit pore, Eq. (1) has to be provided with boundary conditions that utilize known conditions outside the membrane pores. In this section, we will examine the phenomena at the entrance and exit to the pores to obtain these boundary conditions.

Owing to interactions with the pore wall, the concentration of a solute at the pore entrance $x = 0$ changes sharply from its value in the bulk feed solution. This effect can be quantified using an equilibrium partition coefficient $\mathcal{F}$ defined such that:

$$\bar{X}(0) = X_F \mathcal{F} \tag{2}$$

Here, $\bar{X}(0)$ is the solute concentration at the slit pore entrance in direct contact with the solute concentration X_F in the feed stream.

Equation (2) implies an equilibrium treatment of the phenomena at the pore entrance, i.e., the local flow and electric fields at the pore entrance and other perturbations (such as any ongoing adsorption kinetics) cause negligible departures in the cross-distribution of solutes at the pore entrance. For a large solute of Stokes–Einstein radius a and diffusion coefficient $D = 10^{-11}$ m^2/s in a pore of half-width h such that $h - a \sim 10$ nm is the width of the zone accessible to the solute, the characteristic cross-diffusion time is ~10 μs. Nonequilibrium processes have to occur on a longer time scale for the equilibrium approach to be valid; this requirement is satisfied under typical experimental conditions of interest. The wall shear rate for feed channel flow of 1 ml/min is ~0.5 s^{-1} giving a characteristic time scale of ~2 s.[18] Since the average velocity of flow in a pore of length $L = 4$ μm and width $2h \sim 10$ nm at $\Delta P = 2$ psi is ~10 μm/s, the transit time of a solute through the pore is ~0.4 s. The electromigration fluxes due to applied voltages produce field lines parallel to the wall and should not alter the normal distribution of solutes,[41] except in small localized areas of surface charge inhomogeneities.[7] Any inequilibrated adsorption processes at the pore mouth or within the pore is assumed to be on a much slower time scale than the transit time through the pore and is neglected. Small departures from thermodynamic equilibrium are also assumed at pore exits.

The partition coefficient $\mathcal{F}$ characterizes the fact that there is a different probability of finding a solute molecule inside a pore than in the bulk (feed) solution. Detailed methods for calculating $\mathcal{F}$ using various approaches and for various situations of practical interest can be found in the literature.[6,10,45,48] When electrostatic and other long range interactions between a molecule and a pore are weak and the solute molecule is not deformable, $\mathcal{F}$ can be calculated from the fraction of pore area that is geometrically inaccessible to the solute molecule.[10] Over and above this size exclusion effect, factors such as the pore charge, the charge on the solute molecule, presence of electrolyte ions,[48] Van der Waals interactions,[14] concentration effects,[29] molecular deformability[18] etc. can modify the magnitude of $\mathcal{F}$. Specific forms of $\mathcal{F}$ in slit-shaped pores in the presence of size exclusion and electrostatic effects will be necessary in the next section in order to study hemofiltration of proteins using the synthetic nanopore membrane.

Equation (2) provides one of the two boundary conditions needed to calculate the distribution of the solute through Eq. (1), as it is assumed in this work that X_F can be prescribed a value characteristic of the solute mole fraction in the major arteries and arterioles of the blood stream.[34] In an actual experiment with the hemofiltration membrane, the feed solution is preformulated and X_F is known if concentration polarization effects are absent.[53]

For generality, we assume the feed and permeate side to have different partition coefficients $\mathcal{F}$ and $\mathcal{P}$. This is a first step to model all situations where substantially different conditions prevail in the feed and permeate channels. For example, if the feed solution is sufficiently concentrated with a large molecular weight species (which may be the solute itself) the resultant intermolecular repulsion will lead to $\mathcal{P} < \mathcal{F}$.[30] In the absence of significant intermolecular interactions in the feed channel, a situation with $\mathcal{P} < \mathcal{F}$ can also result if attractive interactions are present in the permeate channel. This attractive interaction may result, for example, from the use of a soluble additive in the permeate channel that promotes coagulation of the solute undergoing filtration. Conversely, when the intermolecular interactions in the permeate channel are repulsive, a situation with $\mathcal{P} > \mathcal{F}$ results. The last two situations are of some interest to the RAD operation as different results were obtained[46] depending on whether the permeate channel is perfused with the solvent (PBS solution) or kept solvent-free during the experiments. However, a clear physical understanding of this phenomena is not yet available, although the larger sieving coefficients observed on using a solvent-free permeate side suggests that a situation where $\mathcal{P} < \mathcal{F}$ may have been created in the latter case. The effect of $\mathcal{P}$ on the sieving coefficient is discussed in a following section (section "Concentration Distribution inside a Pore").

A relation similar to $\bar{X}(0) = X_F\mathcal{F}$ is valid at the exit to the pore: $\bar{X}(1) = X_P\mathcal{P}$. However, this relation cannot be used directly as a boundary condition at the channel exit because the value of X_P cannot be prescribed and depends on the permeate flux. We can obtain the second boundary condition by utilizing the continuity of the permeate flux and the solute flux between the pore and the permeate channel as shown below.

The total flux of the solute at the exit of the slit pore should balance the net flux in the permeate stream. The solute concentration in the near-pore region of the permeate channel is assumed to have equilibrated to have a constant but yet unknown value X_P. The net flow efflux through this region must equal the permeate flux $\bar{u}$ through the pore to ensure mass balance

$$J = \bar{u}X_P = \bar{u}\frac{\bar{X}(1)}{\mathcal{P}} \tag{3}$$

Inserting J from Eq. (1b) (evaluated at $x = 1$) into Eq. (3) and rearranging:

$$\left.\frac{\partial \bar{X}}{\partial x}\right|_{x=1} = Pe_H\bar{u}\left(1 + s - \frac{1}{\mathcal{P}K_c}\right)\bar{X}(1) \tag{4}$$

where the new dimensionless parameter:

$$s = \frac{zDE_x^*FK_d}{RT\bar{u}^*K_c} = \frac{zE_x}{Pe_H\bar{u}} \tag{5}$$

incorporates dimensionlessly the effect of any applied/induced electric field (E_x). Asterisks denote dimensional quantities; $E_x^* = RTE_x/(FL)$, $\bar{u}^* = \bar{u}U_0$, $Pe_H = K_cU_0L/K_dD$ and $U_0 = h^2\,\Delta P/(2\,\mu L)$.

The streaming potential effect creates an electric field $E_x < 0$ directed from the permeate toward the feed side of the membrane.[14] The parameter $s > 0$ for transport under the streaming potential of biomolecules like BSA which are negatively charged at physiological pH. Another effect of streaming potential is to reduce the mean velocity of flow $\bar{u}$. Alternatively, external application of an electric field may be explored. If an external electric field $E_x > 0$ directed from the feed toward the permeate side of the membrane is applied, the negatively charged molecules will have $s < 0$.

The equation governing the concentration distribution is summarized below more concisely by inserting Eq. (1b) into Eq. (1a) and utilizing the definition of s:

$$\frac{\partial^2 \bar{X}}{\partial x^2} = Pe_H\bar{u}(1 + s)\frac{\partial \bar{X}}{\partial x} \tag{6}$$

For convenience, from now on, X will signify the distribution of area averaged mole fraction of the solute; we will not further use the bar over X.

Concentration Distribution Inside a Pore

Equation (6) can be solved with the boundary conditions (2) and (4) to give:

$$X(x) = X_F\mathcal{F}\frac{1 + [(1+s)\mathcal{P}K_c - 1]\exp[-Pe_H\bar{u}(1+s)(1-x)]}{1 + [(1+s)\mathcal{P}K_c - 1]\exp[-Pe_H\bar{u}(1+s)]} \tag{7}$$

The sieving coefficient S defined as $X_P/X_F = X(1)/X_F\mathcal{P}$ calculated from this distribution is:

$$S = \frac{(1 + s)\mathcal{F}K_c}{1 + [(1 + s)\mathcal{P}K_c - 1]\exp[-Pe_H\bar{u}(1 + s)]} \tag{8}$$

For a given s in $(-1, \infty)$ the asymptotic forms of Eq. (8) for large and small Pe_H are:

$$S_\infty = \mathcal{F}K_c(1 + s) \quad \text{for } Pe_H \gg 1 \tag{9a}$$

$$S_0 = \frac{\mathcal{F}}{\mathcal{P}} \quad \text{for } Pe_H \ll 1 \tag{9b}$$

A physical interpretation of Eq. (9b) is that any attractive/repulsive interaction in any part of the feed-pore-permeate system biases the Brownian motion to redistribute more/fewer molecules in the zone of attraction/repulsion. It is assumed here apart from Brownian motion, the molecules can respond to the conservative field of an interaction force (such as EDL screened electric field); these two processes near the pore-feed and pore-permeate interfaces determine the value of $\mathcal{F}$ and $\mathcal{P}$. For example, a situation $\mathcal{P} < \mathcal{F}$ will result in feed-pore-permeate molecular distributions that place more molecules in the permeate channel and fewer molecules in the feed channel than the case where $\mathcal{P} = \mathcal{F}$, raising the sieving coefficient S. Also, as discussed by Lazzara and Deen[30] in the context of studying concentration effects on $\mathcal{F}$, the apparent possibility of $S > 1$, if $\mathcal{F}$ is significantly larger than $\mathcal{P}$ is not a contradiction of any fundamental physical principle.

For the transport of negatively charged species like BSA, a negative value of s implies an applied electric field from feed to the permeate side. The case $s = -1$ corresponds to convection being balanced exactly by electromigration and gives rise to a linear concentration distribution that can be obtained by solving Eqs. (4) and (6) directly: $X = X_0\mathcal{F}\left(1 - \frac{Pe_H\bar{u}}{\mathcal{P}K_c + Pe_H\bar{u}}x\right)$. It can be noted, that this distribution and the corresponding sieving coefficient $S = \mathcal{F}\mathcal{P}K_c/(\mathcal{P}K_c + Pe_H\bar{u})$ is independent of K_c since $Pe_H = K_c\bar{u}L/K_dD$, but dependent on K_d.

For $s < -1$, electrostatics dominates convection and $S \to 0$ when $s \ll -1$; this case is of particular interest for solute selectivity as discussed below. At a constant Pe_H, conditions ensuring $(s + 1) \gg 0$ and $(1 + s) \to 0^+$ will also lead to Eqs. (9a) and (9b), respectively.

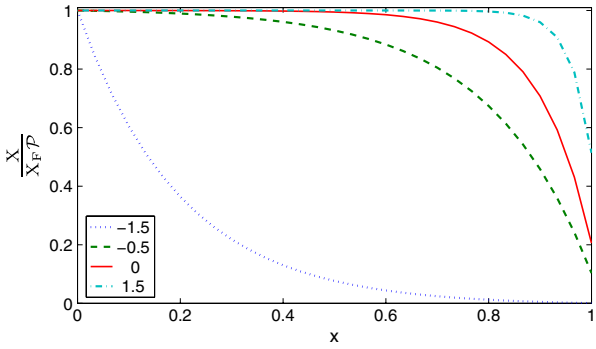


FIGURE 3. Effect of applied and induced electric fields on the concentration distribution in the pore for $Pe_H\bar{u} = 10$ and $\mathcal{F} = \mathcal{P} = 0.8$ studied by prescribing different values −1.5, 0.5, 0, 0.5, 1.5 to the parameter s. For transport of negatively charged solutes, a negative value of s signifies an electric field directed from the feed to the permeate chambers.

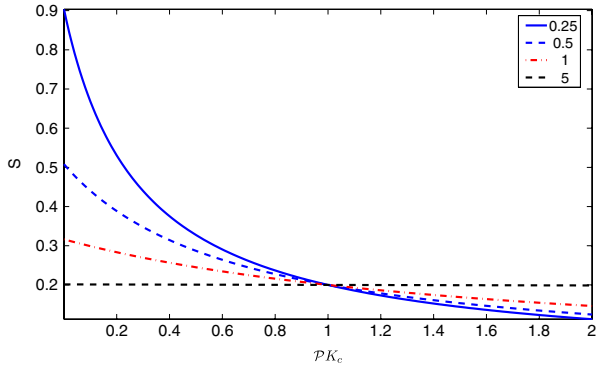


FIGURE 4. Effect of permeate side partition coefficient $\mathcal{P}$ on the sieving coefficient of the pore for $\mathcal{F}K_c = 0.2$, $s = 0$, and $Pe_H\bar{u}$ values 0.25, 0.5, 1, and 5.

The effect of an applied or induced electric field is embodied in the parameter s. Figure 3 examines the concentration distribution for different values of the parameter s. Here $\mathcal{P} = \mathcal{F} = 0.8$ for the curves shown and the sieving coefficient can be read off from this figure as the value of the dependent variable $X(x)/X_F\mathcal{P}$ at $x = 1$. It is clear that the electrostatics dominated case $s = -1.5$ gives a qualitatively different pattern of concentration variation with progressively decreasing slope from the cases with other s values. This suggests that low sieving coefficient for negatively charged solutes can be achieved by applying an electric field directed from the feed to the permeate side.

The sieving coefficient is studied as a function of $\mathcal{P}K_c$ for four values of Pe_H and fixed values of $\mathcal{F}K_c = 0.2$, $s = 0$ in Fig. 4. It is seen that a small value of $\mathcal{P}$ ($\mathcal{P}K_c < 1$) is detrimental to solute selectivity and a large value of $\mathcal{P}$ ($\mathcal{P}K_c > 1$) can enhance solute selectivity. The effect of $\mathcal{P}$ is also less significant for $Pe_H \gg 1$. Large values of Pe_H correspond to high permeate fluxes.

Lowering of sieving coefficient via the enhancement of $\mathcal{P}$ involves rendering exit from the pore unfavorable. One possible strategy is to introduce a solute with large hydrodynamic radius at a high concentration in the solution perfusing the permeate channel. This solute will be called a 'crowding agent' here. The resultant repulsive interactions experienced by a solute undergoing filtration in the bulk of the permeate solution will lead to an increase of $\mathcal{P}$ compared to the situation where the 'crowding agent' is absent. Since the majority of serum proteins are negatively charged at physiological pH, a negative charge on the crowding agent can further enhance the selectivity. To achieve high concentrations, it is desirable that the crowding agent has a reasonably high solubility in PBS. It should also have a large molecular radius to ensure good crowding and to minimize back-diffusion from the permeate to the pore. A sulfate of a high molecular weight dextran such as dextran 200 with a negative charge and a diameter of 20 nm is a possible candidate for the 'crowding agent,' though further investigation is necessary. It can be noted here that presence of similar concentration-based effects in the feed solution leads to an increase of the sieving coefficient through an increase of $\mathcal{F}$ in Eqs. (9a) and (9b). See for example, Lazzara and Deen[31] for the effect of BSA on the sieving coefficient of BSA itself and that of Ficoll. On the other hand use of coagulants in the permeate channel will be detrimental to the sieving in small pores (in low Pe_H situations) lowering $\mathcal{P}$ and raising S, as evident from Eqs. (8) and (9b).

Equation (8) and Fig. 4 suggest that the sieving coefficient has a different pattern of dependence on exit conditions as represented by $\mathcal{P}$ than on the entrance conditions as represented by $\mathcal{F}$. A possible way to exploit the fact that sieving coefficient decreases with increasing $\mathcal{P}$ is to introduce large quantities of a high molecular weight soluble solute in the permeate solution at the start of an experiment. However, this effect can be significant only when Pe_H is small or in other words, the membrane is not operating at its full convective capacity.

It can be noted that in Figs. 3 and 4, for better representation of the parameter space and controls, the effect of electric field on the flow field (electroosmotic flow) is ignored; this would correspond to a negligible charge on the pore walls. It is fairly straightforward to incorporate an electroosmotic flow in the model for $\bar{u}$; this is covered in context of predicting the streaming potential effect in the next section.

APPLICATION TO HEMOFILTRATION

In order to study hemofiltration by the synthetic nanopore membrane, the specific forms of $\mathcal{F}$ and $\mathcal{P}$ are necessary. Two situations are of interest: (a) when

molecules behave as hard spheres geometrically restricted by the pore (steric partitioning) and (b) the pore and molecule interact by long range Coulombic forces (electrostatic partitioning). Steric partitioning is appropriate when both the pore and the solutes are uncharged or carry charges that are screened completely by an EDL that is thinner than the shortest distance between the pore walls and the solute.[14,44] Electrostatic partitioning is appropriate for calculating $\mathcal{F}$ (or $\mathcal{P}$) if both the pore and the EDL carry charges and are only partial screened by their respective EDL of finite width.

Forces shorter in range than the electrostatic force, such as colloidal dispersion forces, are excluded from modeling consideration in the following discussions on the expectation that the former are superseded in magnitude by the latter although progress in representing these forces has been achieved in other contexts.[4,56] In the remainder of this article, we will concentrate on slit-shaped pores and situations where $\mathcal{F} = \mathcal{P}$, unless mentioned otherwise.

Steric Partitioning

For a spherical particle entering a slit pore (Fig. 2d), if the solution outside the pore is sufficiently dilute to neglect intermolecular interactions and if there are no significant electrostatic or other long-range interactions between the solute molecules and the pore wall, geometrical as well as thermodynamic considerations can be used to derive[10]

$$\mathcal{F} = \mathcal{P} = 1 - \chi \tag{10}$$

where $\chi = a/h$ is the ratio of the solute radius (a) to the pore half-width (h).

For a spherical particle moving inside a slit pore under pressure-driven flow (Fig. 2d), the hindrance factors K_c and K_d are evaluated by studying the motion of a spherical particle placed within the slit and involve calculation of the hydrodynamic flow field and the drag force on the particle[10,19] and accounting for the size exclusion on the walls. The expressions for K_c and K_d are as follows[9]:

$$K_c = \frac{1 - 3.02\chi^2 + 5.776\chi^3 - 12.3675\chi^4 + 18.9775\chi^5 - 15.2185\chi^6 + 4.8525\chi^7}{1 - \chi} \tag{11a}$$

$$K_d = \frac{1 + \frac{9}{16}\chi\log(\chi) - 1.19358\chi + 0.4285\chi^3 - 0.3192\chi^4 + 0.08428\chi^5}{1 - \chi} \tag{11b}$$

These expressions for K_c and K_d do not involve the 'centerline approximation,' i.e., the requirement that the particle migrates along the centerline of the channel that is present in expressions from the older literature.[10]

Electrostatic Partitioning

If the molecule suffers a change $\Delta G = G_{pore} - G_{feed}$ in its Gibb's free energy on entering the pore, the partition coefficient $\mathcal{F}$ can be calculated using[10,48]:

$$\mathcal{F} = \overline{\exp\left(-\frac{\Delta G}{RT}\right)} = \frac{1}{2}\int_{-1+a/h}^{1-a/h} \exp\left(-\frac{\Delta G}{RT}\right) dy \tag{12}$$

where $y = y^*/h$ and the solute center cannot occupy $|y| \geq a/h$. Note that Eq. (10) can also be obtained as a special case of Eq. (12), by choosing $\Delta G = 0$.

The Gibb's free energy change ΔG_{sp} due to electrostatic interaction when a charged plate (p) and a spherical solute (s) approach each other from infinite separation can be calculated using[14,23]

$$\begin{aligned}\frac{\Delta G_{sp}}{RT} = {} & \frac{\pi a I}{\kappa^2}\left[(\zeta_p F/RT)^2 + (\zeta_s F/RT)^2\right] \\ & \times \left(\frac{2\zeta_p\zeta_s}{\zeta_p^2 + \zeta_s^2}\log\left(\frac{1 + \exp(-\kappa(h-a))}{1 - \exp(-\kappa(h-a))}\right)\right. \\ & \left. - \log\left[1 - \exp(-2\kappa(h-a))\right]\right) \\ \zeta_p = {} & \epsilon_e\kappa\sigma_p \\ \zeta_s = {} & \frac{\epsilon_e\sigma_s a}{1 + \kappa a}\end{aligned} \tag{13}$$

Here, σ_p, σ_s and ζ_p, ζ_s are the surface charge density and zeta potential values at the plate surface and solute surface. I is the ionic strength measured by $I = 1/2\sum z_i^2 c_i$ where c_i and z_i are the concentrations and valences of the ith electrolyte ion. The Debye–Hückel parameter κ is the inverse of the Debye length $\lambda = \sqrt{\epsilon_e RT/IF^2}$.

Equation (13) is based on the Derjaguin approximation and formally requires $\kappa a \gg 1$ and $H \ll a$ where

$H = h - a$ is the shortest distance between the solute and the plate for its validity. Under this condition, only a small region of the sphere near its point of closest approach to the plate takes part in the interaction. The Derjaguin approximation can be interpreted as a geometrical substitution of the sphere with a paraboloid of revolution closely fitting the sphere in the region near the point of closest approach with the plate.[39] Equations (13) also assumes constant surface charge density during the interaction, i.e., no additional charge transfer occurs across any of the solid–electrolyte interfaces involved when the solute and the plate (or pore wall) approach each other. Equations (13) are formally applicable only when $|\zeta F/RT|$ is small, as a linearization of the Poisson–Boltzmann distribution was assumed in its derivation[23] in order to maintain analytical tractability. In what follows, PBS will be treated as a sodium chloride solution of the corresponding ionic strength for simplicity, because the density of like charged ions like hydrogenphosphate and dihydrogenphosphate anions in the EDL of a negatively charged surface is small.[27]

To calculate the interaction energy between a slit and a sphere, we use the Derjaguin model and further assume that the EDL on the two pore walls do not interact with each other. This approximation appears reasonable since the largest Debye length and the smallest pore width of interest are of 8 Å (in 0.143 M PBS) and 70 Å, respectively; good electrostatic screening is thus ensured by the small ratio of EDL and pore sizes. The solute can be replaced by two paraboloids interacting separately with the nearest plate. Thus, the Gibbs free energy change when a slit pore and a single spherical solute moves from infinite separation to the pore-solute configuration of interest can be calculated by adding the Gibbs free energy change of two separate paraboloid-plate pairs, each given by Eq. (13). The ΔG for a sphere within a slit nanopore for use in Eq. (12) can, therefore be approximated by $2\Delta G_{sp}$.

Use of the centerline approximation,[10] which is (at least) expected to be very accurate for solutes that fit tightly into pores[9] leads to the following simplified version of Eq. (12):

$$\mathcal{F} = \exp\left(-\frac{\Delta G}{RT}\right)(1-\chi) \tag{14}$$

Equation (14) suggests that the partition coefficient is factorizable into a purely electrostatic effect (the first factor) and a purely steric effect (the second factor, c.f. Eq. 10) in the centerline approximation.

Despite the several levels of approximations involved, unlike point charge based approaches,[11] an electrostatic partitioning calculation based on Eqs. (13) and (14) incorporates the coupled effects of electrolyte salt concentration and solute size through the self-capacitance/self-energy (multipliers of ζ^2 in Eq. 13) and mutual capacitance (multipliers of $\zeta_p\zeta_s$) of the interacting geometries and charge screening by the electrolyte (terms with κh) of the EDL. The conditions $H = h - a \gg a$ and $\kappa a \gg 1$ required for the Derjaguin approximation, correspond to the desirable design principles of the hemofilter: small pore sizes to filter large molecules at high (physiological) ionic strengths. Thus, the physical detail in the current model is comparable to similar first principle models for a sphere within a cylinder.[43,48] Electrostatic models based on the Debye–Hückel approximation[45] have provided a reasonable representation of experimental data on the effect of ionic strength on sieving coefficients in membranes with cylindrical pores. The Derjaguin approximation has been successful in explaining experimental data on the force of interaction between atomic force microscope tip and a flat surface and between colloidal particles.[55] However, in cases where the conditions required for the formal validity of Derjaguin($h - a \ll a$, $\kappa a \gg 1$) and Debye–Hückel approximations ($\zeta F/RT \gg 1$) are not met, quantitatively accurate conclusions from this electrostatic model should not be expected.

In summary, given the zeta potentials ζ_p and ζ_s and/or the surface charge densities σ_p and σ_s and the solution ionic strength I, the partition coefficient $\mathcal{F}$ between a charged pore wall and solute can be calculated, when charges on both are partially screened by its EDL. The same considerations apply at the exit of the pore for the calculation of $\mathcal{P}$.

The hindrance factors K_c and K_d are assumed to be unchanged from the values calculated by Eq. (11) during electrostatic interaction.[43] From Eqs. (9a) and (14), the sieving coefficient in the high convective flux limit ($Pe_H \gg 1$) under electrostatic partitioning is:

$$S = \exp\left(-\frac{2\Delta G_{sp}}{RT}\right)(1-\chi)K_c \tag{15}$$

where K_c is given by Eq. (11a), subject to the validity of all the assumptions described above.

Sieving of Polydisperse Solutes: Effect of Partitioning at Pore Exit

In Fig. 5, the filtration of polydisperse Ficoll 70 (M_w = 10–70 kDa) is studied theoretically for a 10 nm membrane utilizing Eqs. (8), (10) (only for $\mathcal{F}$) and (11a). Here, M_w stands for the 'weight averaged molecular weight' of Ficoll, as obtained for example by gel permeation chromatography.[2] A purely pressure-driven flow responding to a pressure gradient of 2 psi is used. Under this conditions, the Pe_H values are not

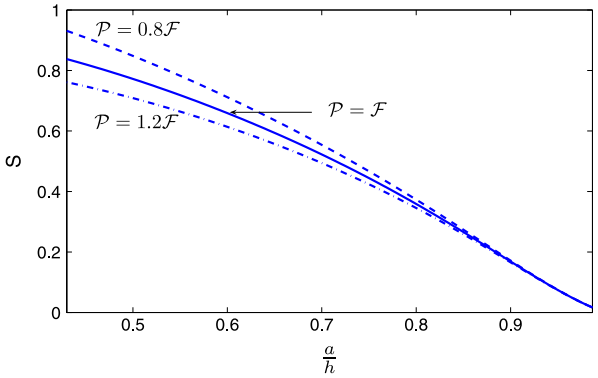


FIGURE 5. Theoretically calculated sieving coefficients of polydisperse Ficoll 70 (M_w = 10–70 kDa and a = 21–49 Å) in a pore of fixed width ($2h$ = 10 nm) under three different conditions on the permeate side corresponding to $\mathcal{P} = 1.2\mathcal{F}$, $\mathcal{P} = \mathcal{F}$, and $\mathcal{P} = 0.8\mathcal{F}$ (dashed line). Refer to text for a discussion on how these curves can provide a possible explanation of the relative magnitudes of sieving coefficients observed in experiments with PBS-free and PBS-wetted permeate side conditions.

large (varying between 0.5 and 0.8 depending on D for a particular Ficoll 70 size) and any difference in $\mathcal{P}$ and $\mathcal{F}$ continues to affect the sieving coefficient calculated by Eq. (8). A correlation $a(\text{Å}) = 0.421\ (M_w\ (\text{Da}))^{0.427}$ suggested by Venturoli and Rippe[51] is used for calculating the radii of Ficoll 70 from M_w and the diffusion coefficients are obtained using the Stokes-Einstein relationship.[10] The solid curve corresponds to an experiment with similar conditions at the entrance and exit, $\mathcal{F} = \mathcal{P}$. The dashed and dotted curve correspond to an experiment in which $\mathcal{P} = 0.8\mathcal{F}$ and $\mathcal{P} = 1.2\mathcal{F}$. It is seen that the selectivity deteriorates (sieving coefficient increases) for $\mathcal{P} = 0.8\mathcal{F}$ and improves for $\mathcal{P} = 1.2\mathcal{F}$ at all values of Ficoll 70 radius. Roy and Fissell[46] have observed that when the permeate side of the membrane is kept dry the sieving coefficients increases from the standard case where the permeate side is kept perfused in PBS solution throughout the experiment. Figure 5 offers a possible qualitative explanation for the raised sieving coefficient when the permeate side is kept dry if it is accepted from a phenomenological perspective that in the case of permeate side being dry $\mathcal{F} - \mathcal{P}$ is larger than when the permeate side is wetted.

More work is necessary to understand the physics of the permeate side partitioning, such as the role of air–PBS interfaces formed and to represent quantitatively the experimental data observed,[46] which possibly involves simultaneous effects of the permeate-side conditions raising the sieving coefficient for all fractions with deformation of Ficoll 70 affecting the large radii fractions.[18] Transients originating from the dilution of the permeated solute by the preexisting solution in the wetted channel may also lead to smaller observed sieving coefficients with a wetted permeate side than with a dry permeate side, regardless of the relative magnitude of $\mathcal{F}$ and $\mathcal{P}$. Under this condition Eq. (4) is inapplicable and this effect is currently under investigation.

Streaming Potential

The mechanism of flow generation in the hemofiltration experiments of Fissell *et al.*[18] is a pressure-drive of ΔP across the membrane. Recalling that $U_0 = h^2\Delta P/2\,\mu\text{L}$, this immediately suggests the flow distribution in the pore to be a classical Poiseuille flow: $u \simeq (1 - y^2)$. However, it can be anticipated from the small size of the pore and the presence of charges on both the pore and the solute that the streaming potential effect[14] can play a role. In view of this fact and for the purpose of generality, we take the flow in a nanopore of the hemofiltration membrane to be driven by the combined action of a transmembrane pressure and a constant applied or induced (due to streaming potential) electric field. This electric field results in an electroosmotic component to the flow. In case of the streaming potential effect, the electroosmotic component is directed oppositely to the pressure-driven flow.

The ratio γ compares the characteristic electroosmotic velocity scale $\epsilon_e E_x^* RT/F\mu$ to the pressure-driven velocity scale U_0:

$$\gamma = \frac{\epsilon_e RTE_x^*}{FU_0\mu} \tag{16}$$

Here ϵ_e is the electrical permittivity and $h^2\Delta P/8\,\mu\text{L}$. Here, and in all later instances, the asterisk (*) is used as a superscript to differentiate a dimensional variable from the corresponding dimensionless variable.

If the zeta potential ζ^* on the pore wall is nondimensionalized by the potential scale $\phi_0 = RT/F$, the dimensionless flow field in the slit-shaped nanopore (see Fig. 2d) is given by[32]:

$$u = 1 - y^2 - \gamma(\zeta - \phi) \tag{17a}$$

$$\bar{u} = \frac{2}{3} - \gamma(\zeta - \bar{\phi}) \tag{17b}$$

The ζ potential is negative for the silica surface used in the hemofiltration membrane at physiological pH. The electric potential ϕ due to the EDL on the silica surface averaged across the channel is $\bar{\phi}$. Since $\bar{\phi} \leq \zeta$, the electroosmotic component of the flow cannot exceed $|\gamma\zeta|$. In the absence of any applied electric field, γ is negative due to the effect of streaming potential and the electroosmotic component is oppositely directed to the pressure-driven component. The ratios s and γ can be used to characterize the effect of an externally applied electric field as well as streaming potentials.

The electric field due to the streaming potential is oppositely directed to the flow ($E_x < 0$). The protein BSA is negatively charged; this means that $zE_x > 0$ leading to $s > 0$ in Eq. (9a). Consequently, Eq. (9a) would appear to predict an increase in the sieving coefficient if the factor $\mathcal{F}$ is unaltered. It can be noted here that electrostatic repulsions between the wall and the molecule can also lead to a competing effect that results in a reduction of $\mathcal{F}$, as discussed in section "Electrostatic Partitioning".

The streaming field is given by[14]:

$$E_x^* = \frac{\epsilon_e \zeta^* \Delta P}{\Lambda_0 L} \tag{18}$$

where $\Lambda_0 = c_{NaCl}(D_{Na} + D_{Cl})F^2/RT$ is the conductivity based on the feed solution salinity and the diffusion coefficients $D_{Na} = 1.33 \times 10^{-9}$ m^2/s and $D_{Cl} = 2.03 \times 10^{-9}$ m^2/s of sodium and chloride ions.[8] The thickness of the membrane L is 4 μm (c.f. Fig. 2). The above expression does not account for the overlap of EDL; however, accounting for the EDL overlap always leads to a reduction in the streaming electric field from that predicted by Eq. (18).[32] Equation (18) can therefore be trusted to provide a conservative estimate of the electric field (E_x^*), electromigration of the solute (s) and the electroosmotic backflow component (γ) of $\bar{u}$.

Using a zeta potential -40 mV on the channel walls and $c = 0.143$ M, the parameters s and γ were found to be 3% and 0.004% for transmembrane pressures of 2 psi, on using Eq. (18) in the definition of s and (16). The value 40 mV used for the zeta potential is based on the experimental measurements of Min *et al.*[38] on a fused silica surface with 0.01 M potassium-phosphate buffered saline. Since (a) the PBS ionic strength of 0.143 M in the hemofiltration device is more than 10 times this value and zeta potential decreases with ionic strength[27] and (b) the hemofiltration device employs a polyethylene glycol coating which inhibits zeta potential,[49] it can be concluded that the values of s and γ calculated here using $\zeta = -40$ mV will not be exceeded during the experiments. Thus, the effect of streaming potential is negligible at the salt concentrations present in the feed solution for the hemofiltration device.[18]

Experimental Comparison

Sieving coefficients were measured for the proteins carbonic anhydrase (CA), bovine serum albumin (BSA), and thyroglobulin (Fig. 7). The proteins (Carbonic Anhydrase, M_w 29 kD; No. C3934, Sigma), bovine serum albumin (Bovine Serum Albumin, M_w 69 kD; No. A5378, Sigma), and Thyroglobulin (M_w 670 kD; No. T1001, Sigma) were dissolved at 500 μg/mL concentration in one of the following two solutions: 0.143 M PBS, 1.43 M PBS. Experiments were also performed with bovine whole blood anticoagulated with ACD-A citrate. A custom built cross-flow filtration system (Fig. 6) housing a membrane of the same design as shown in Fig. 2a was used. Membranes with pore widths of 7, 9.69, 10.9, 12.78, 42 nm as inferred from hydraulic permeability measurements[18] were used. The pore walls of all membranes, except the 42 nm membrane were surface-modified with poly(ethylene glycol), using a previously reported solution phase method,[40] modified to omit all sonication steps and continuing the PEG deposition for 12 h. The retentate side of the membrane was perfused at a flow rate of 1 mL/min from a 100 mL reservoir of feed solution, and the permeate side of the membrane was wetted with a measured volume of PBS (unless mentioned otherwise below). Compressed dry air was used to generate the transmembrane pressure (2 psi) which was monitored by a pressure transducer within the filtration cell (Entran, EPX 10PG, Les Clayes-sous-Bois, France). The ultrafiltration volume was monitored in a calibrated syringe barrel (Hamilton, Reno, Nevada) capped with parafilm. After testing, membranes were removed from the filtration cell, rinsed with deionized water, dried, and examined for adherent thrombus by scanning electron microscopy. Gel permeation chromatography (GPC) with an Ultrahydrogel 500 column was used to analyze feed and permeate samples. A 600E controller and either a 474 fluorescence detector (Waters Corp., Milford, MA) or an Agilent 1200 HPLC system was used for detection was used for GPC. Further details on the experimental methods[17] and apparatus[18] are available elsewhere.

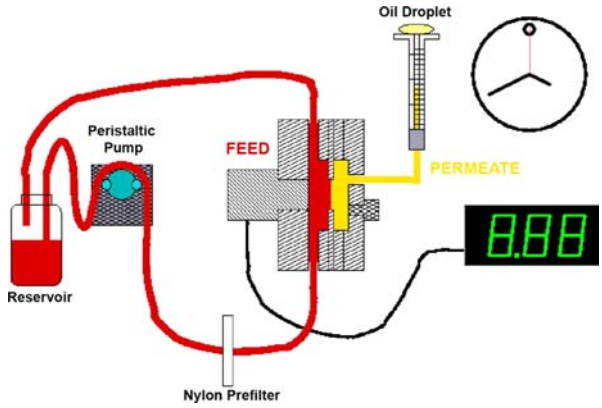


FIGURE 6. The ultrafiltration setup used in the experiments. A membrane of same design as in Fig. 2a separates the feed chamber from the permeate chamber. See also Fissell *et al.*[18]

The largest sources of quantitative errors in the experimental data originate in the accurate measurement of the volume of solution filtered by the membrane given that the permeate solution is pre-wetted with PBS in most experiments as well in the silver staining and densitometry steps of protein detection by gel

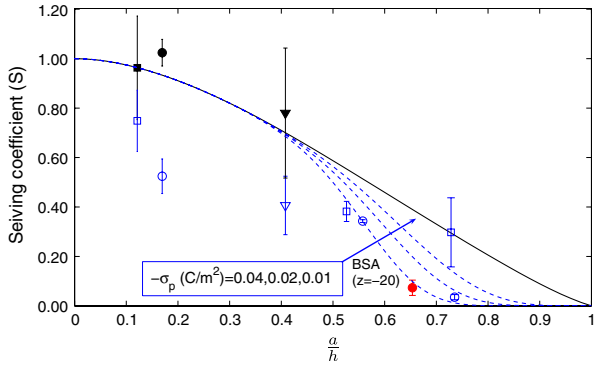


FIGURE 7. Experimental sieving coefficients of bovine serum albumin (BSA), thyroglobulin, and carbonic anhydrase (CA) in 1× PBS, 10× PBS, and bovine blood with clotting factors removed as a function of the ratio *a*/*h* of protein hydrodynamic radius (*a*) and pore half-width (*h*) and comparison with theoretical curves obtained under the assumption of steric partitioning (solid curve) and electrostatic partitioning as applicable to bovine serum albumin (dashed curves). The shape of the symbols indicate the type of protein: circles, triangles, and square stand for BSA, thyroglobulin, and CA, respectively. All data in 1× PBS feed solution is indicated with hollow symbols, the data in 10× PBS is indicated with solid symbols colored black, the only datum in blood (also identifiable uniquely by a horizontal coordinate value of *a*/*h* = 0.65) is indicated with a solid symbol colored red. The dashed curves are obtained using a charge number of −20 for BSA and for three different values of surface charge ($\sigma = -0.01, 0.02, 0.04$ C/m^2) density on the pore walls in Eqs. (13) and (15). The experiments were conducted in membranes with the following pore-widths (2*h*): 7, 9.69, 10.9, 12.78, and 42 nm.

permeation chromatography. This has resulted in the large standard deviations in some of the data reported. The fact that the sieving coefficient is greater than unity for BSA in the 42 nm membrane with 10× PBS most likely originates from these experimental errors.

The theoretical model used below for experimental comparison will assume $\mathcal{F} = \mathcal{P}$; the only experimental situation reported here where this assumption may not be accurate in principle is the 12.7 nm membrane where the permeate reservoir was drained before the experiment. Equation (9a) with $s = 0$ is used to obtain the theoretical sieving curve for sterically excluded solutes shown as a solid line in Fig. 7. Finite Peclet number effects can result in larger observed sieving coefficients than that predicted by this equation, especially in small pores and for small molecules. It was checked by using Eq. (8) in place of Eq. (9a) that the resultant increase in the sieving coefficient is within 16% of the single standard deviation experimental uncertainty (Fig. 2) in case of CA in the 7 nm membrane, the situation with the smallest $Pe_H \simeq 2$. The solute radius needed for calculating $\chi = a/h$ are calculated assuming molecular weights 29, 67, and 670 kDa for CA, BSA, and thyroglobulin and using the correlation $a(\text{Å}) = 0.483\ [M_w\ (\text{Da})]^{0.386}$ suggested for calculating Stokes–Einstein radius of globular proteins.[51] The effects of streaming potential and concentration polarization[18] were neglected.

The data for CA in 7 and 42 nm pores using 10× PBS and PBS solutions, respectively, agree very well with predictions based on steric partitioning model (solid curve in Fig. 7) calculated using Eq. (9a). A general trend in the experimental data for all three proteins is that the sieving coefficient in 10× PBS is always larger than in PBS, other conditions remaining the same; a possible reason for this is stronger electrostatic effects in the latter. The sieving coefficients of BSA are consistently overestimated by the steric partitioning model. Since the BSA molecule is expected to carry significant negative charges[42] at the pH = 7.4 of the experiments, electrostatic effects were investigated.

The BSA data in the 9.69, 10.9, 12.78, and 42 nm pores show a reasonable agreement with the predictions from the electrostatic model (the dashed curves in Fig. 7) calculated using Eq. (15), particularly when a σ_p lying between −0.02 and −0.04 C/m^2 or ζ_p lying between −23.2 and −46.5 mV (according to the second of Eq. 13) and a charge number −20 for BSA[42] and standard properties of dilute aqueous electrolytes at room temperature are used in Eq. (13). The zeta potential values required appear to be larger than expected of PEG coated silica in 0.143 M PBS. However, as shown in Fig. 7, the use of lower surface charge density values, such as $\sigma_p = -0.01$ C/m^2 (or $\zeta_p = -11.6$ V) do not change the qualitative features of the electrostatic partitioning curves. The bovine blood used for BSA filtration experiment with the 10.9 nm membrane appears to possess electrostatic behavior similar to 1× PBS. Further, the electrostatic model (not shown in Fig. 7) with $z = -4$[20] and $a = 25.5$ Å[51] and $\sigma = -0.04$ C/m^2 could also be used to represent the CA datum (square symbol) in the 9.69 nm pore ($\chi = a/h = 0.53$) within the corresponding experimental uncertainty. This is the only CA sieving datum, for which electrostatic interactions appears to have a significant role.

The measured sieving coefficient values in 1× PBS for the largest pore, 42 nm are smaller than that can be predicted by the electrostatic (as well as steric) model. A plausible explanation for this observation is provided below.

The PEG coating was not applied to the 42 nm channel. Bare silica surfaces are known to promote protein adsorption. Through protein adsorption on the channel walls, the effective cross-section of the channel might have been reduced.[50] Taking a thickness of 110 Å[3,13] for an adsorbed layer of thyroglobulin, the reduction in the effective pore width due to a single layer of thyroglobulin adsorbed on one of the pore surfaces normal to the smallest dimension of the pore (cross-stream surface) will shift the effective abscissa to

$a/h = 0.55$, explaining the measured sieving coefficient either through steric or electrostatic models within the limits of experimental error. A reduction in pore size equivalent to five 30 Å thick[1,22] adsorbed layers of BSA on each cross-stream surface will relocate the effective abscissa of the corresponding experimental data points to $a/h = 0.6$ allowing the steric model to explain the sieving coefficient within the limits of experimental error. The thickness of the protein layers are estimated based on the reported crystalline structure[3,22] assuming the molecules lie with their longest dimension parallel to the pore wall (side-on orientation[1]). Similarly, two layers of end-on adsorption (thickness of each layer, 55 Å[26]) or three layers of side-on adsorption (thickness of each layer, 40 Å[26]) of carbonic anhydrase on each wall can explain the observed sieving behavior of the CA datum near $a/h = 0.1$ in 1× PBS and the 42 nm membrane. In solutions of high ionic strength, adsorbed layers of proteins are known to be destabilized,[21,25] so we speculate that the adsorbed layer(s) are absent in 10× PBS. This explains why this effect appears only in the 1× PBS solution. If no adsorption is assumed, electrostatic interaction alone also produces a similar relative trend in sieving coefficients between 10× PBS and 1× PBS,[44] but considering that the Debye screening length in 1× PBS is ~7 Å, this effect is quantitatively minimal in channels as wide as 42 nm.

The BSA datum in the 42 nm membrane and 10× PBS is a marginal outlier showing a sieving coefficient (averaged over three observations) greater than unity, to which no clear explanation beyond the experimental errors mentioned before is evident. Like other data collected using the same membrane, the relative position of this datum with respect to the 1× PBS BSA datum for the same protein is consistent with the expectation of lower protein adsorption, lower electrostatic interaction and/or a lower degree of hydration in 10× PBS than in 1× PBS, of which, a quantitative significance appears to be ascribable only to the first-mentioned factor, as discussed in detail earlier in the section.

CONCLUSIONS

The simultaneous effects of applied electric fields, transmembrane pressures, entrance, and exit partitioning phenomena on the pore level concentration distributions and sieving coefficients in a nanopore membrane has been studied with a hindered transport model. Two important and new predictions from this model are that solute selectivity can be improved by: (a) applying an electric field (c.f. the case with $s = 1.5$ in Fig. 3) directed from the feed toward the permeate channel and (b) by establishing conditions that impede the exit of solute from the pore (increasing $\mathcal{P}$) leads to lower sieving coefficients i.e. improved solute selectivity (c.f. Fig. 4). These two predictions can serve as a basis for new experimental approaches, such as application of voltages through electrodes inserted in the feed and permeate channels and the use of crowding agents in the permeate solution.

The theoretical model is then specialized to understanding the permeability and selectivity characteristics of the hemofiltration membrane for the RAD. Approximate but closed form expressions for electrostatic interaction and partition coefficient in slit pores are developed for the first time in the literature. The streaming potential effect is found to have negligible effect on the flow rate as well as solute transport through the nanopores under typical RAD operating conditions.

Data on filtration of proteins by the hemofiltration membrane for the RAD have been reported and compared with the theoretical predictions customized to the RAD hemofilter. Protein filtration data in 10× PBS solutions and the data on the filtration of carbonic anhydrase in 7 and 42 nm membranes are consistent with steric partitioning of spheres with the ratio of diameter to pore size calculated with Stokes–Einstein radii; the theoretical predictions for the last two cases being quantitatively accurate without the requirement of any adjustable parameter. The data for BSA in 1× PBS and bovine blood is consistent with the presence of electrostatic interactions. The observed values of sieving coefficient in the membrane with the widest pore (42 nm) which was not coated with PEG using the most dilute solution of interest (1× PBS) was smaller than the theoretical predictions, to which a plausible explanation based on protein adsorption has been forwarded.

The sieving coefficient values obtained experimentally from the current generation of the RAD as well as from model predictions ($O(1\%)$ for CA) are considerably higher than that required ($O(10^{-2}\%)$) to replace the glomerular function of protein rejection in a biological kidney $O(10^{-2}\%)$.[24] Therefore, additional strategies to improve solute selectivity such as further reduction of pore size and/or enhancement of the electrostatic interactions between charged solutes and charged pores through surface modifications should be explored in the future work. More fundamental understanding and more accurate predictions of sieving behavior of Ficoll 70, the effect of solvent/ion attachment to proteins during filtration and the physical phenomena in the permeate side of the membrane are also necessary. The model for electrostatic partitioning also needs to be generalized to high surface charge densities, large Debye layer thicknesses and large plate separation to enable more quantitative prediction on sieving coefficients under a wide variety of experimental conditions.

Theoretical as well as experimental consideration of the long-term hemocompatibility of PEG coated membrane surfaces, effects of protein adsorption and subsequent conformational changes[5,37,54] on membrane permeability, selectivity and *in vivo* performance need to be characterized. More work on the role of non-electrostatic factors such as Van der Waals force, hydrogen bonding, and Lewis-acid–Lewis-base interactions on partitioning as well as nonspecific adsorption during hemofiltration is necessary.[28] The role of nonequilibrium phenomena such as fluid skimming in the transport of solutes also need future consideration.[52] All of these effects will be investigated in the future work. More robust validation of the theoretical model through additional experimental comparison is necessary before the model developed can be used for predictive or design purposes. This will be done as more experimental data becomes available. Model development as well as experiments for characterizing the membrane performance with respect to filtration of other molecules in blood such as β_2-microglobulin, creatinine, inulin, and urea as well as important probe solutes such as Ficoll 70 and dextrans will also be conducted in our future work.

ACKNOWLEDGMENTS

The project described was supported by NIH Grant Number R01EB008049 from the National Institute of Biomedical Imaging and Bioengineering. The content is solely the responsibility of the authors and does not necessarily represent the official views of the National Institute of Biomedical Imaging and Bioengineering or the National Institutes of Health. The authors thank Prof. Andrew L. Zydney (AZ) of Pennsylvania State University for reviewing the manuscript and for helpful suggestions. The writing and model development for this paper was principally undertaken by SD under guidance from TC and additional guidance from SR and AZ; the experimental results were contributed by WHF and SR.

CLEVELAND CLINIC DISCLOSURE POLICY

Co-authors, WHF and SR, are inventors on one or more patents related to the subject material in this paper, and are entitled to a share of any royalty payments that may derive from commercialization of the patent(s).

REFERENCES

[1]Asanov, A. N., L. J. Delucas, P. B. Oldham, and W. W. Wilson. Heteroenergetics of bovine serum albumin adsorption from good solvents related to crystallization conditions. *J. Colloid Interf. Sci.* 191(1):222–235, 1997.

[2]Baltus, R. E., and J. L. Anderson. Hindered diffusion of asphaltenes through microporous membranes. *Chem. Eng. Sci.* 38(12):1959–1969, 1983.

[3]Bloth, B., and R. Bergquis. The ultrastructure of human thyroglobulin. *J. Exp. Med.* 128(5):1129–1136, 1968.

[4]Brant, J. A., and A. E. Childress. Membrane-colloid interactions: comparison of extended DLVO predictions with AFM force measurements. *Environ. Eng. Sci.* 19(6): 413–427, 2002.

[5]Brash, J. L., and S. Uniyal. Dependence of albumin-fibrinogen simple and competitive adsorption on surface properties of biomaterials. *J. Polym. Sci.* 66:377–389, 1979.

[6]Brenner, H., and L. J. Gaydos. The constrained Brownian movement of spherical particles in cylindrical pores of comparable radius. *J. Colloid. Interf. Sci.* 58(2):312–356, 1977.

[7]Chen, L., and A. T. Conlisk. Effect of nonuniform surface potential on electroosmotic flow at large applied electric field strength. *Biomed. Microdevices* 11(1):173–181, 2009.

[8]Cussler, E. L. Diffusion: Mass Transfer in Fluid Systems. Cambridge University Press, 1997.

[9]Dechadilok, P., and W. M. Deen. Hindrance factors for diffusion and convection in pores. *Ind. Eng. Chem. Res.* 45(21):6953–6959, 2006.

[10]Deen, W. M. Hindered transport of large molecules in liquid-filled pores. *Am. Instit. Chem. Eng. J.* 33(9):1409–1422, 1987.

[11]Deen, W. M., B. Satvat, and J. M. Jamieson. Theoretical model for glomerular filtration of charged solutes. *Am. J. Physiol. Renal Physiol.* 238(2):126–139, 1980.

[12]Deen, W. M., M. J. Lazzara, and B. D. Myers. Structural determinants of glomerular permeability. *Am. J. Physiol. Renal. Physiol.* 281:579–596, 2001.

[13]Deshpande, V., and S. G. Venkatesh. Thyroglobulin, the prothyroid hormone: chemistry, synthesis and degradation. *Biochim. Biophys. Acta (BBA)/Protein Struct. Mol. Enzymol.* 1430(2):157–178, 1999.

[14]Elimelech, M. Particle Deposition and Aggregation: Measurement, Modelling and Simulation. Butterworth-Heinemann, 1998.

[15]Fissell, W. H., and H. D. Humes. Tissue engineering renal replacement therapy. In: Tissue Engineering and Artificial Organs, edited by J. D. Bronzino. Boca Raton, Florida: CRC Press, 2006, pp. 60-1–60-14.

[16]Fissell, W. H., H. D. Humes, S. Roy, and A. Fleischman. Ultrafiltration membrane, device, bioartificial organ, and methods, May 23 2006. US Patent 7,048,856.

[17]Fissell, W. H., A. Dubnisheva, A. N. Eldridge, A. J. Fleischman, A. L. Zydney, and S. Roy. High-performance silicon nanopore hemofiltration membranes. *J. Membrane Sci.* 326(1):58–63, 2009.

[18]Fissell, W. H., S. Manley, A. Dubnisheva, J. Glass, J. Magistrelli, A. N. Eldridge, A. J. Fleischman, A. L. Zydney, and S. Roy. Ficoll is not a rigid sphere. *Am. J. Physiol. Renal Physiol.* 293(4):F1209–F1213, 2007.

[19]Ganatos, P., R. Pfeffer, and S. Weinbaum. A strong interaction theory for the creeping motion of a sphere between plane parallel boundaries. Part 2. Parallel motion. *J. Fluid Mech. Digital Arch.* 99(04):755–783, 2006.

[20]Gao, J., F. A. Gomez, R. Harter, and G. M. Whitesides. Determination of the effective charge of a protein in solution by capillary electrophoresis. *Proc. Natl. Acad. Sci. USA* 91(25):12027, 1994.

[21]Green, J. S., and J. W. Jorgenson. Minimizing adsorption of proteins on fused silica in capillary zone electrophoresis by the addition of alkali metal salts to the buffers. *J. Chromatogr.* 478(1):63–70, 1989.
[22]He, X. M., and D. C. Carter. Atomic structure and chemistry of human serum albumin. *Nature* 358(6383):209–215, 1992.
[23]Hogg, R., T. W. Healy, and D. W. Fuerstenau. Mutual coagulation of colloidal dispersions. *Trans. Faraday Soc.* 62:1638–1651, 1966.
[24]Humes, H. D., W. H. Fissell, and K. Tiranathanagul. The future of hemodialysis membranes. *Kidney Int.* 69:1115–1119, 2006.
[25]Jones, K. L., and C. R. O'Melia. Protein and humic acid adsorption onto hydrophilic membrane surfaces: effects of pH and ionic strength. *J. Membrane Sci.* 165(1):31–46, 2000.
[26]Karlsson, M., L. G. Martensson, B. H. Jonsson, and U. Carlsson. Adsorption of human carbonic anhydrase II variants to silica nanoparticles occur stepwise: binding is followed by successive conformational changes to a molten-globule-like state. *Langmuir* 16(22):8470–8479, 2000.
[27]Kirby, B. J., and E. F. Hasselbrink. Zeta potential of microfluidic substrates: 1. Theory, experimental techniques, and effects on separations. *Electrophoresis* 25(2):187–202, 2004.
[28]Kurrat, R., J. E. Prenosil, and J. J. Ramsden. Kinetics of human and bovine serum albumin adsorption at silica–titania surfaces. *J. Colloid Interf. Sci.* 185(1):1–8, 1997.
[29]Lazzara, M. J., D. Blankschtein, and W. M. Deen. Effects of multisolute steric interactions on membrane partition coefficients. *J. Colloid Interf. Sci.* 226(1):112–122, 2000.
[30]Lazzara, M. J., and W. M. Deen. Effects of plasma proteins on sieving of tracer macromolecules in glomerular basement membrane. *Am. J. Physiol. Renal Physiol.* 281(5):860–868, 2001.
[31]Lazzara, M. J., and W. M. Deen. Effects of concentration on the partitioning of macromolecule mixtures in agarose gels. *J. Colloid Interf. Sci.* 272(2):288–297, 2004.
[32]Levine, S., J. R. Marriott, G. Neale, and N. Epstein. Theory of electrokinetic flow in fine cylindrical capillaries at high zeta-potentials. *J. Colloid Interf. Sci.* 52(1):136–149, 1975.
[33]Lopez, C. A., D. G. Attiah, A. J. Fleischman, S. Roy, and T. A. Desai. Evaluation of silicon-based micro- and nanostructured environments on neurosecretory cells. *Biomaterials* 27:3075, 2006.
[34]Martini, F. Fundamentals of Anatomy and Physiology, 5th edn. Prentice Hall International Inc., 2001.
[35]Matsubara, S., K. Okabe, K. Ouchi, Y. Miyazaki, Y. Yajima, H. Suzuki, M. Otsuki, and S. Matsuno. Continuous removal of middle molecules by hemofiltration in patients with acute liver failure. *Crit. Care Med.* 18(12):1331, 1990.
[36]Mehta, A., and A. L. Zydney. Permeability and selectivity analysis for ultrafiltration membranes. *J. Membrane Sci.* 249(1–2):245–249, 2005.
[37]Michel, R., S. Pasche, M. Textor, and D. G. Castner. Influence of PEG architecture on protein adsorption and conformation. *Langmuir* 21(26):12327–12332, 2005.
[38]Min, J. Y., D. Kim, and S. J. Kim. A novel approach to analysis of electroosmotic pumping through rectangular-shaped microchannels. *Sens. Actuators B Chem.* 120(1): 305–312, 2006.
[39]Ohshima, H., and T. Kondo. Electrostatic interaction of an ion-penetrable sphere with a hard plate: contribution of image interaction. *J. Colloid Interf. Sci.* 157(2):504–508, 1993.
[40]Papra, A., N. Gadegaard, and N. B. Larsen. Characterization of ultrathin poly (ethylene glycol) monolayers on silicon substrates. *Langmuir* 17(5):1457–1460, 2001.
[41]Patankar, N. A., and H. H. Hu. Numerical simulation of electroosmotic flow. *Sens. Actuators B* 20:103–110, 1994.
[42]Peters, T. All About Albumin: Biochemistry, Genetics and Medical Applications. Academic Press, Inc., 1996.
[43]Pujar, N. S., and A. L. Zydney. Electrostatic and electrokinetic interactions during protein transport through narrow pore membranes. *Ind. Eng. Chem. Res.* 33(10):2473–2482, 1994.
[44]Pujar, N. S., and A. L. Zydney. Charge regulation and electrostatic interactions for a spherical particle in a cylindrical pore. *J. Colloid Interf. Sci.* 192(2):338–349, 1997.
[45]Pujar, N. S., and A. L. Zydney. Electrostatic effects on protein partitioning in size-exclusion chromatography and membrane ultrafiltration. *J. Chromatogr. A* 796:229–238, 1998.
[46]Roy, S. and W. H. Fissell, 2008 (Private communication).
[47]Scherrer, R., and P. Gerhardt. Molecular sieving by the *Bacillus megaterium* cell wall and protoplast. *J. Bacteriol.* 107(3):718–735, 1971.
[48]Smith, F. G., and W. M. Deen. Electrostatic double-layer interactions for spherical colloids in cylindrical pores. *J. Colloid Interf. Sci.* 78:444–465, 1980.
[49]Smith, J. T., and Z. El Rassi. Capillary zone electrophoresis of biological substances with surface-modified fused silica capillaries with switchable electroosmotic flow. *J. High Resolut. Chromatogr.* 15(9):573–578, 1992.
[50]Striemer, C. C., T. R. Gaborski, J. L. Mcgrath, and P. M. Fauchet. Charge-and size-based separation of macromolecules using ultrathin silicon membranes. *Nature (London)* 445(7129):749–753, 2007.
[51]Venturoli, D., and B. Rippe. Ficoll and dextran vs. globular proteins as probes for testing glomerular permselectivity: effects of molecular size, shape, charge, and deformability. *Am. J. Physiol. Renal Physiol.* 288(4):605–613, 2005.
[52]Yan, Z. Y., A. Acrivos, and S. Weinbaum. Fluid skimming and particle entrainment into a small circular side pore. *J. Fluid Mech. Digital Arch.* 229:1–27, 2006.
[53]Zeman, L. J. and A. L. Zydney. Microfiltration and Ultrafiltration: Principles and Applications. CRC Press, 1996.
[54]Zhang, M., and M. Ferrari. Hemocompatible polyethylene glycol films on silicon. *Biomed. Microdevices* 1(1):81–89, 1998.
[55]Zhmud, B. V., A. Meurk, and L. Bergström. Evaluation of surface ionization parameters from AFM data. *J. Colloid Interf. Sci.* 207(2):332–343, 1998.
[56]Zydney, A. L., and N. S. Pujar. Protein transport through porous membranes: effects of colloidal interactions. *Colloid Surface A* 138(2–3):133–143, 1998.